

Interfacial Pressure and Viscoelasticity of Antibodies and Their Correlation to Long-Term Stability in Formulation

Kiet G. Pham, Benjamin R. Thompson, Tingting Wang, Shayak Samaddar, Ken K. Qian,* Yun Liu, and Norman J. Wagner*



Cite This: *J. Phys. Chem. B* 2023, 127, 9724–9733



Read Online

ACCESS |



Metrics & More

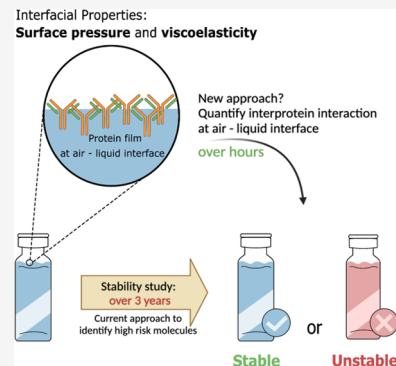


Article Recommendations



Supporting Information

ABSTRACT: Monoclonal antibodies (mAbs) form viscoelastic gel-like layers at the air–water interface due to their amphiphilic nature, and this same protein characteristic can lead to undesired aggregation of proteins in therapeutic formulations. We hypothesize that the interfacial viscoelasticity and surface pressure of mAbs at the air–water interface will correlate with their long-term stability. To test this hypothesis, the interfacial viscoelastic rheology and surface pressure of five different antibodies with varying visible particle counts from a three-year stability study were measured. We find that both the surface pressures and interfacial elastic moduli correlate well with the long-time mAb solution stability within a class of mAbs with the interfacial elastic moduli being particularly sensitive to discriminate between stable and unstable mAbs across a range of formulations. Furthermore, X-ray reflectivity was used to gain insight into the interfacial structure of mAbs at the air–water interface, providing a possible molecular mechanism to explain the relationship between interfacial elastic moduli and the long-term stability.



1. INTRODUCTION

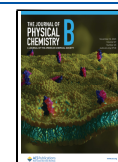
Monoclonal antibodies (mAbs) are considered as the leading group of therapeutics for treating a variety of diseases, including human cancers and autoimmune disorders.¹ While they are potent therapeutics, their intrinsic aggregation tendency brings a longstanding issue to biopharmaceutical production and storage.² Non-native aggregation in solution, i.e., aggregation for which the protein loses its native form, is thought to proceed by exposure of hydrophobic groups through fluctuations in the quaternary structure or partial unfolding, leading to protein–protein aggregation that can result in nucleates, which grow to micron-sized aggregates visible to the naked eye.² The presence of visible aggregates diminishes the therapeutic efficacy and can trigger undesired immunogenic responses in patients. This could lead to drug tolerance or life-threatening complications such as autoimmunity to endogenous protein.³ As a result, regulatory agencies strictly regulate the amount of visible aggregates in therapeutic protein formulations.³

Assessing the stability of mAbs, i.e., particulate formation propensity during product development, requires significant time, effort, and expense. It commonly takes 24–36 months of study to determine the particulate formation tendency of new protein therapeutics.⁴ Therefore, rapid screening tools to help identify high-risk molecules during drug development are highly desired. Predicting this long-term stability early in the development process by identifying potentially unstable formulations is of critical importance. One example is the parallel temperature initial rate (PTIR) method to determine

the aggregation rate as a function of temperature by Barnett et al.⁵ From this, one can extrapolate the aggregation rate at storage temperatures via the Arrhenius relationship.^{5,6} However, over a longer time scale (i.e., years), the non-Arrhenius kinetic behavior becomes significant, which leads to large uncertainty in the extrapolated results.^{5–7} Hydrogen–deuterium exchange measurements in proteins, which probes conformational fluctuations that expose buried hydrophobic moieties in proteins in lyophilized formulations, have shown to correlate with long-term stability for myoglobin.⁸ Simulation methods have also been employed; Chennamsetty et al. developed a parameter called spatial aggregation propensity (SAP) to determine the dynamic exposure of aggregation-prone regions.⁹ However, it could be argued that the assumption that aggregation-prone sequences are solvent-exposed and able to interact with neighboring proteins is not always valid under different formulation conditions.¹⁰

There are several studies demonstrating the connection between the solution stability and the interfacial properties of proteins. Shieh et al. report that an initial increase in surface pressure as mAbs adsorb at an air–water interface is a good predictor for agitation-induced aggregation.¹¹ In addition, by

Received: August 31, 2023
Revised: October 17, 2023
Accepted: October 18, 2023
Published: November 2, 2023



comparing three food proteins, bovine serum albumin (BSA), β -lactoglobulin, and lysozyme, Mitropoulos et al. show that less stable proteins form higher shear modulus films at the air–water interface.¹² Monoclonal antibodies strongly bind to air–water interfaces, which result in high surface pressures.^{13,14} Adsorption to the air–water interface can be via flat-on, end-on, or side-on configurations, with the crowding and orientation leading to β -sheet formation at the surface.^{14,15} Thus, adsorbed mAbs can form networks that give rise to an interfacial layer with significant shear rheological properties at the air–water interface.^{16,17}

Motivated by these findings, we hypothesize that the interfacial viscoelasticity and the surface pressure of therapeutic monoclonal antibodies can provide an indication of long-term protein stability in solution. This hypothesis is not based on a mechanism of the air–water interface providing nucleates for visible particle formation in solution, but rather, the rationale is that the high protein concentration and local organization in molecular orientation at the hydrophobic air–water interface will act to catalyze interprotein interactions in hours under similar thermal and buffer conditions that lead to visible particles forming in formulation over years of quiescent storage. To test this hypothesis, we utilized surface tensiometry, interfacial rheology, and X-ray reflectometry to investigate the relationship between the solution long-term stability and the air–water interfacial properties and structure of a set of monoclonal antibodies of similar origin.

2. METHODS

2.1. Materials. Five mAbs were supplied by Eli Lilly & Company. MAbs A and B belong to the IgG1 family and mAbs C, D, and E belong to the IgG4 family. Antibodies A, B, C, and E are monoclonal antibodies with a molecular mass of approximately 150 kDa. Antibody D is a bispecific mAb with a molecular mass of approximately 200 kDa. These mAbs are supplied in a concentrated stock solution of approximately 50 mg/mL in various buffers that are tabulated in Table S1 (Supporting Information). The stock solutions were diluted to a concentration of 0.75 ± 0.02 mg/mL by using the same pH and ionic strength buffer as the stock solution. Prior to all interfacial characterization measurements, a fresh protein solution was prepared and filtered through a 200 nm pore size cellulose filter, and their concentration was confirmed to be 0.75 ± 0.02 mg/mL with UV–visible spectroscopy (Nanodrop 2000 Spectrophotometer) by measuring the absorbance at a wavelength of 280 nm. Milli-Q water was used in all experiments (resistivity = $18.2 \text{ M}\Omega\cdot\text{cm}^{-1}$). Surfactant Poloxamer 188 (P188) was not included in the protein sample for interfacial characterization because it will mask all intrinsic interfacial properties and prevent protein adsorption, as shown and discussed in Figure S6 in the Supporting Information.

2.2. Dynamic Surface Tensiometry. The dynamic surface tension was measured using a KSV NIMA Langmuir trough with dimensions of 317 mm length and 75 mm width along with a Pt–Ir Wilhelmy plate. Before any measurements, the trough was sequentially cleaned with soapy water, ethanol, acetone, 2-propanol, and water and finally dried with compressed air. The Wilhelmy plate was flame-cleaned to remove any leftover residues. The trough was filled with the appropriate buffer (~ 150 mL), and the surface tension of buffer, γ_0 , was recorded as 72.8 ± 0.2 mN/m at room temperature (22 ± 2 °C). The surface pressure was then set to

zero, followed by the aspiration of the buffer solution. The trough was then filled with the same volume of filtered protein solution (0.75 mg/mL). The dynamic surface pressure $\Pi(t)$ (mN/m) of the protein solution was monitored with a decrease in surface tension over time. The surface pressure $\Pi(t)$ is calculated as

$$\Pi(t) = \gamma_0 - \gamma(t)$$

where $\gamma(t)$ is the surface tension of the protein solution over time. A humidifier with a feedback loop was used to maintain a relative humidity of 75% to minimize evaporation. The surface pressure was monitored for 2 h.

2.3. Interfacial Shear Rheology. To probe the shear rheological properties, a stress-controlled rheometer Discovery HR-3 was used along with double-walled ring (DWR) geometry. The characteristic length of the DWR geometry is 0.7 mm, which has shown an advantage in decoupling the momentum contribution of the bulk from the interface (i.e., increasing the Boussinesq number).¹⁸ An oscillatory time sweep at a strain, γ , of 0.1% and an angular frequency, ω , of 5 rad/s followed by a frequency sweep ($\gamma = 0.1\%$, $\omega = 0.1$ –100 rad/s) were performed to characterize the protein layer at the air–water interface. The chosen strain amplitude ensured the measurements were performed in the linear viscoelastic regime (LVR) as shown in the Supporting Information. The Pt–Ir ring was washed with ethanol, acetone, isopropanol, and water and was flamed with a butane torch before any measurements. The Delrin trough was also thoroughly cleaned with ethanol, acetone, isopropanol, and water prior to any measurements. Once a protein sample was loaded into the Delrin trough, the ring was aligned to the interface to perform the measurement. The sample trough is mounted on a Peltier plate to maintain the experimental temperature at 22 °C. The time sweeps were chosen to be performed over 8 h. A humidifier was used to suppress the evaporation over the duration of the experiment. The reported data is the average between independent runs of 5 independent samples.

2.4. Long-Term Stability of Antibodies. Five antibody molecules (A–E) were prepared in formulation conditions as shown in Table S1. Since they are not in final drug product formulations, they are not isotonic. All formulations contain 25 mg/mL antibody and 0.04% Poloxamer 188 (P188). After formulations were prepared and filled into 5 mL type I glass vials with 3 mL fill, they were incubated at 5 °C up to about 3 years. Stability was mainly monitored by visual inspection of all time points and background membrane imaging (BMI) for the last time point (with more details in the Supporting Information).

2.5. X-ray Reflectometry. X-ray reflectivity (XRR) measurements (D8 Advance reflectometer, Bruker AXS) with an X-ray wavelength, λ , of 1.542 Å from the Cu–K α radiation with a minimum resolution of $\Delta\lambda = 0.004$ Å and $\Delta\theta = 0.0003$ radians or $\Delta Q = 0.0025 \text{ \AA}^{-1}$ were performed using a Teflon Langmuir trough in an enclosed chamber on a vibration isolation stage. The XRR data were measured as a function of incident angle θ over the momentum transfer vector perpendicular to the surface, $Q = (4\pi/\lambda) \sin(\theta)$. The Q -range covered was 0.015 – 0.52 \AA^{-1} . All of the measurements were carried out at room temperature (22 ± 2 °C). Each XRR scan took a total of three hours for sample alignment and data acquisition.

Before the samples were loaded into the Langmuir trough (width = 100 mm, length = 320 mm), the trough was cleaned

sequentially with ethanol, acetone, isopropanol, and water. Protein solutions were prepared (0.75 mg/mL), filtered, and then loaded into the clean trough (total volume \sim 230 mL) so that there was a positive meniscus. Prior to X-ray reflectivity data acquisition, the samples were allowed to equilibrate for 2.5 h to allow for protein adsorption, unfolding, and rearrangement at the air–water interface.

2.6. X-ray Reflectivity Data Reduction and Analysis.

XRR data was reduced by *Reductus* and analyzed using *ReflID* and the DREAM algorithm.¹⁹ A slab model was implemented to fit the reflectivity data to obtain the electron density profile (EDP) as a function of interfacial depth. The best fit was chosen based on the minimum χ^2 parameter. All of the protein reflectivity data were fitted using a four-slab model, where each layer has a thickness, roughness, and scattering length density. The amount of adsorbed protein, i.e., total volume fraction of mAbs, φ_{total} , at the air–water interface was calculated by integrating the volume occupancy (VO) profile along the interfacial depth and normalized by the interfacial thickness as described elsewhere.^{16,20}

For further verification of the features obtained from the slab model, a Hermite spline method was utilized to fit the reflectivity data. The Hermite spline model provides more freedom to model and extract more details from complex biomolecular architectures such as monoclonal antibodies at the air–water interface while still maintaining physically valid conditions. More details about the Hermite spline model can be found elsewhere.²¹ A Monte Carlo Markov Chain method was used to determine the uncertainties of the fits from which the SLD profile and volume occupancy profile are also determined with their confidence band.²² The similarity in the EDP (as shown in Figure S7 in the Supporting Information) obtained from two different fitting models, i.e., slab model and Hermite spline model, provide increased confidence in the obtained volume occupancy profiles calculated from the XRR data.

3. RESULTS AND DISCUSSION

3.1. Protein Long-Term Stability.

The number of aggregates was quantified by using background membrane imaging (BMI), and the number of $>25 \mu\text{m}$ aggregates for each mAb is presented in Figure 1. The stable or low particulate formation propensity mAbs have a lower number of $>25 \mu\text{m}$ aggregates from the long-term stability study and vice versa. mAbs B and C have a lower number of $>25 \mu\text{m}$ aggregates as compared to the other antibodies and are classified as stable mAbs in this study. A comprehensive stability study over this 36 month time period by visual inspection and background membrane imaging (BMI) is provided in the Supporting Information (p S-6), showing that the visible particles appear only after some time period. P188 was also added to the formulations to mitigate the interfacial stresses to the mAbs by blocking adsorption to air–liquid and silicon oil–liquid interfaces.^{23,24} Recent studies from Dixit et al. and Zhang et al. show that there are no observable interactions between P188 and mAbs other than preventing the adsorption of mAb to the interfaces.^{25,26} Therefore, the formation of aggregates can mainly be attributed to interprotein interactions in solution. The use of P188 may not fully eliminate interfacial stress from silicon oil contamination arising from the vial stoppers, as discussed by Grapentin et al.²⁷ However, the interfacial behavior of mAbs at a silicon oil–water interface is consistent with that of an air–water interface, as demonstrated

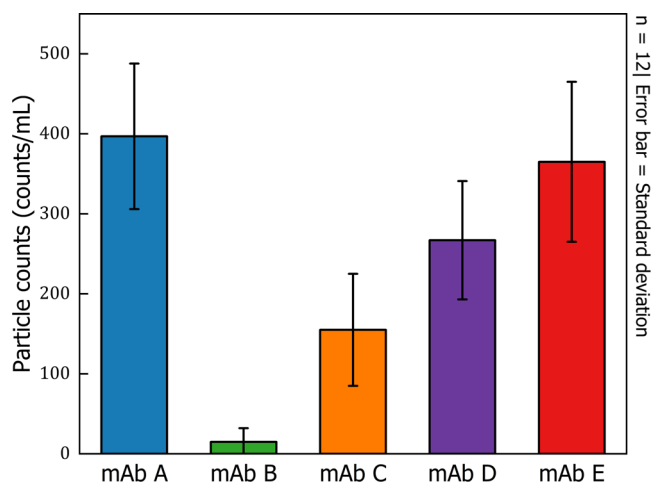


Figure 1. Number of $>25 \mu\text{m}$ aggregates from a three-year stability measurement quantified by background membrane imaging (BMI). The mAb solutions were stored at 25 mg/mL at 5 °C under quiescent conditions over three years. The reported particle counts are the average of 12 replicates for one vial and the error bars are the standard deviation.

in studies by Shieh et al. and Kannan et al.^{11,28,29} Based on these results, we hypothesize that the interfacial properties of mAbs measured at the air–water interface may correlate with the long-term particulate formation propensity of mAbs in solution containing both P188 and contamination by silicon oil. The number of $>25 \mu\text{m}$ particles from BMI is particularly important as the study by Kannan et al.²⁴ suggested that the formation of insoluble aggregates is relevant to the cohesive network or the viscoelasticity of the film at the air–liquid interface.

3.2. Surface Tensiometry.

Due to their amphiphilic nature, mAbs strongly adsorb to the air–liquid interface and thereby increase surface pressure (Figure 2). Initially, in the first 30 min, the surface pressure rapidly increases as mAb molecules adsorb to the air–liquid interface. This significant change in surface pressure is usually referred to as “the rapid fall region” in terms of surface tension by Hua et al.³⁰ Once the

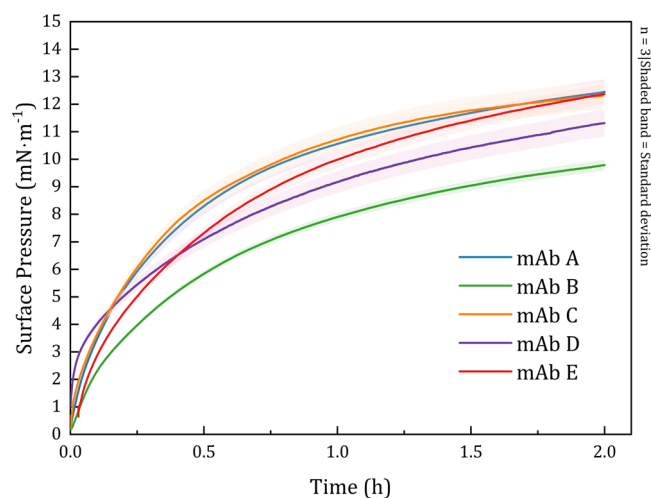


Figure 2. Representative surface pressure profiles for all five mAbs over 2 h at 22 ± 2 °C. The concentration of protein solution is 0.75 mg/mL. The shaded band is the standard deviation of three individual measurements.

Table 1. Tabulated Interfacial Characteristics and Stability of mAb at the Air-Liquid Interface

mAb	>25 μm particle counts (counts/mL)	2 h surface pressure ($\text{mN}\cdot\text{m}^{-1}$)	average interfacial elastic modulus ($\text{Pa}\cdot\text{m}$)	total volume fraction ϕ_{total}	hydrophobic volume fraction $\phi_{\text{hydrophobic}}$
A	397 \pm 91	12.8 \pm 0.4	0.0498 \pm 0.0074	0.242 \pm 0.025	0.88 \pm 0.04
B	17 \pm 19	9.9 \pm 0.3	0.0237 \pm 0.0069	0.208 \pm 0.015	0.80 \pm 0.05
C	155 \pm 70	12.2 \pm 0.2	0.0333 \pm 0.0051	0.253 \pm 0.015	0.83 \pm 0.03
D (bispecific)	267 \pm 74	11.5 \pm 0.5	0.0947 \pm 0.0131	0.235 \pm 0.014	0.91 \pm 0.04
E	365 \pm 77	12.4 \pm 0.5	0.0486 \pm 0.0036	0.243 \pm 0.025	0.86 \pm 0.04

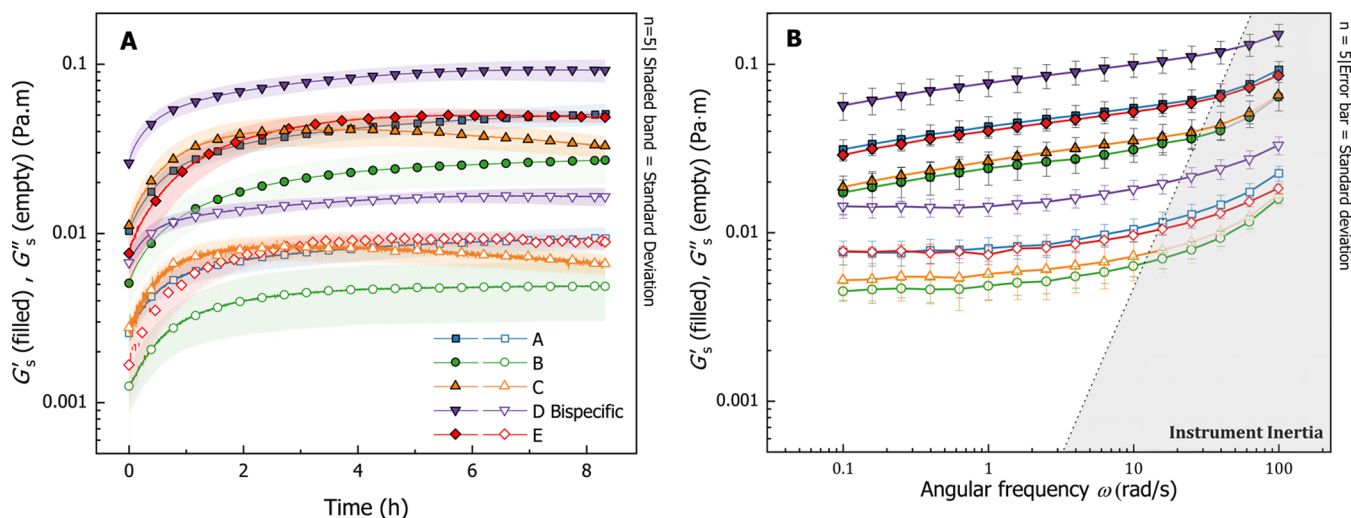


Figure 3. Interfacial rheological properties of mAb solutions (labeled with five different colors) with the concentration of 0.75 mg/mL and salt concentration NaCl < 0.7 mM at 22 °C. The filled and empty symbols represent interfacial elastic modulus G'_s and viscous modulus G''_s , respectively. (A) Oscillatory time sweep over 8.3 h with oscillatory strain, $\gamma_{s,\omega}$ of 0.1% and frequency, ω , of 5 rad/s. The shaded bands represent the standard deviation of the five individual measurements. (B) Frequency sweep at the end of 8.3 h of time sweep with the oscillatory strain $\gamma_{s,\omega}$ of 0.1% and frequency from 0.01 to 100 rad/s. The error bars represent the standard deviations of five measurements. The shaded gray area indicates when the instrument inertia becomes significant and the data in this regime will show an increase due to this effect.

interface is saturated with protein, the relative change in the surface pressure becomes smaller. This continual, but gradual, increase in surface pressure is attributed to the continued densification and conformational changes of the densely packed mAbs at the interface.²⁴ The data plotted in Figure 2 are averages over three independent measurements, and the shading represents standard deviations; the surface pressure values at $t = 2$ h are tabulated in Table 1. These 2 h surface pressures are compared to the >25 μm particle counts from the long-term stability study in Figure 4A. It is imperative to recognize that as the bulk concentration increases beyond the critical bulk concentration, the interfacial properties of the protein interface are weakly dependent on the bulk concentration as discussed by Lin et al.³¹ For mAb at the air–water specifically, Kanthe et al. identified 0.5 mg/mL as the critical bulk concentration because there are no major discrepancies in interfacial properties and structure found at the higher concentration.¹⁴ Therefore, it is reasonable to correlate the interfacial properties at a bulk concentration of 0.75 mg/mL to the solution stability result measured at the bulk concentration of 25 mg/mL. While the differences in surface pressures are relatively small ($\sim 25\%$ across the series), the surface pressures increase systematically with long-term >25 μm particle counts in solution across the 5 mAbs. A simple linear trend has an R^2 of 0.85, indicating a strong correlation between the surface pressure and the long-term solution stability. In other words, the less stable mAb (higher particle counts) yields a higher surface pressure after 2 h. However, the

95% confidence band (Figure 4A) of this empirical correlation is large such that this measurement is not sufficiently sensitive for a screening tool for mAb solution stability.

3.3. Interfacial Shear Rheology. Interfacial rheology provides a related but more sensitive probe of the adsorbed mAb layer as it depends directly on the strength of the interactions between adsorbed proteins as well as the amount of adsorbed protein. Protein adsorbed at an air–water interface can be categorized as a complex fluid–fluid interface.³² In addition to the isotropic surface tension, a thermodynamic property that primarily depends on surface concentration, the protein film can be characterized by extra surface stress arising from the viscoelastic nature of the adsorbed layer.³³ Interfacial small-amplitude oscillatory shear (SAOS) measurements are carried out in the linear viscoelastic regime, where properties are measured without disturbing the interface.³⁴ In these measurements, an oscillatory strain (γ_s) is applied based on the frequency (ω) and strain amplitude ($\gamma_{s,0}$)³⁴

$$\gamma_s(t) = \gamma_{s,0} \sin(\omega t)$$

The sinusoidal stress response is composed of a combination of purely elastic and viscous responses. For viscoelastic materials in the LVR, the interfacial stress response can be decomposed into an interfacial elastic (storage) modulus G'_s and viscous (loss) modulus G''_s as

$$\sigma_s(t) = \gamma_{s,0} [G'_s(\omega) \sin(\omega t) + G''_s(\omega) \cos(\omega t)]$$

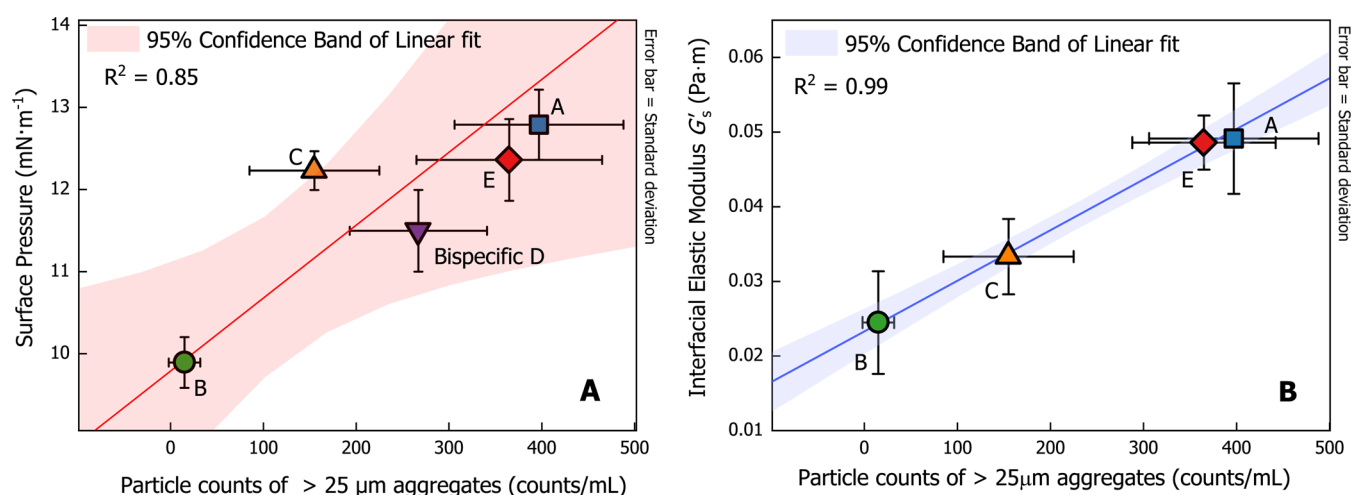


Figure 4. Empirical correlations between interfacial properties and >25 μm particle counts from the long-term stability study. (A) Linear fit between 2 h surface pressures and particle counts of mAbs (labeled in 5 colors). The red line is the linear fit with $R^2 = 0.85$, and the red band represents the 95% confidence band of the linear fit. (B) Linear fit between interfacial elastic modulus G'_s (calculated by averaging out data points over the final hour from the oscillatory time sweep in Figure 3B) and visible particle counts of four mAbs (excluding bispecific antibody D). The blue line is the linear fit with $R^2 = 0.99$, and the blue band represents the 95% confidence band of the linear fit.

Oscillatory time sweep measurements were performed at 0.1% strain amplitude, which is in the LVR for all samples, to probe the dynamic surface shear rheological properties over 8.3 h (30,000 s). Although the surface pressure (Figure 2) marginally changed after 2 h, the surface viscoelasticity was still evolving, and therefore, experiments were performed at 8.3 h. While longer experiments are possible, this was viewed to be long enough to establish the trends in the data without incurring significant errors due to evaporation or surface contamination.³⁵

Similar to the surface pressure, the results for the surface elastic and viscous moduli rise rapidly as mAbs adsorb and then evolve more slowly as shown in Figure 3A. The initial, high rate of increase is attributed to the adsorption, and the evolution is related to the structural rearrangements of mAb to the air–water interface.²⁴ After the first hour, the rate of change is much slower as the adsorption kinetics becomes slower for the dense adsorbed layer and mAbs at the interface rearrange and form specific interactions.¹⁴ The data plotted are averages over five independent experiments, with the shading representing the standard deviation.

Importantly, the elastic modulus, G'_s , is much greater in magnitude than the viscous modulus, G''_s , which indicates that the protein interfacial layer is primarily elastic solid-like and not fluid-like as might be expected for only weakly interacting molecules adsorbed at the interface. Over time, the strength of the mAb interfacial film continually increases as shown by the increase in magnitude of G'_s , except for mAb C, which shows a slight decrease in modulus after ~4 h. After 6 h, the change in G'_s and G''_s slows dramatically for all mAbs, which suggests that the conformational change, reorientation, and densification occurring within the protein interfacial layer have also slowed.^{14,16} The time evolution of the linear viscoelastic moduli is observed to be slightly different for each mAb, which could be attributed to the intrinsic molecular structure, intermolecular interactions in the dense, adsorbed layer, and the formulation condition of each mAb.

To further characterize the nature of the interfacial layer, a frequency sweep is carried out immediately after the oscillatory time sweep. The frequency sweep is performed in the linear

regime at an oscillatory strain of 0.1% and a frequency ranging from 0.01 to 100 rad/s. The results, plotted in Figure 3B, confirm the primarily elastic nature of the interface, typical of a polymer or protein gel. The interfacial elastic modulus, G'_s , is approximately an order of magnitude greater than the interfacial viscous modulus, G''_s , and over the measured frequency range, the moduli are only weakly dependent on frequency, typical of soft glassy materials.³⁶ Moreover, the strain amplitude sweep in Figure S1 (Supporting Information) does not show a maximum in G''_s immediately beyond the yield,³⁷ confirming that the adsorbed mAb layer at the air–water interface exhibits soft glassy rheological properties.^{38,39} The soft glassy characteristics are consistent with a densely adsorbed layer of mAbs at the air–water interface.^{14,17} The interfacial layers for all five mAbs exhibit interfacial elastic moduli on the order of magnitude of 1×10^{-2} Pa·m. From neutron and X-ray reflectivity, the mAb layers have a thickness, δ , on the order of magnitude of 10^2 Å.^{14,16,40} An estimate of the equivalent bulk elastic modulus $G' = G'_s/\delta$ yields $\sim 10^6$ Pa.³⁹ This indicates that the mAb interfaces so formed have very significant elastic moduli that would not be observed for molecules that simply adsorb to the interface with only weak interactions.^{16,24,41} It should be noted that these interfacial rheological properties are significantly different from the Newtonian rheological properties of the mAbs in bulk solution at the low solution concentration of 0.75 mg/mL.¹⁶

It is also noteworthy that the interfacial rheologies of all five mAb solutions have a nearly identical frequency dependence, as illustrated by the similarity of $\tan \delta$ shown in Figure S2 (Supporting Information). Thus, the major difference between these mAb interfaces is the magnitude of interfacial moduli G'_s and G''_s , which reflects differences in the strength of protein–protein interactions at the air–water interface that is most likely driven by the partial unfolding of proteins at the interface. A stronger interprotein attraction yields a more elastic interfacial film.

The average interfacial elastic (or storage) modulus is averaged over the final hour of the time sweep (tabulated in Table 1), and the results are compared to the >25 μm particle counts from the three-year stability study. A clear correlation

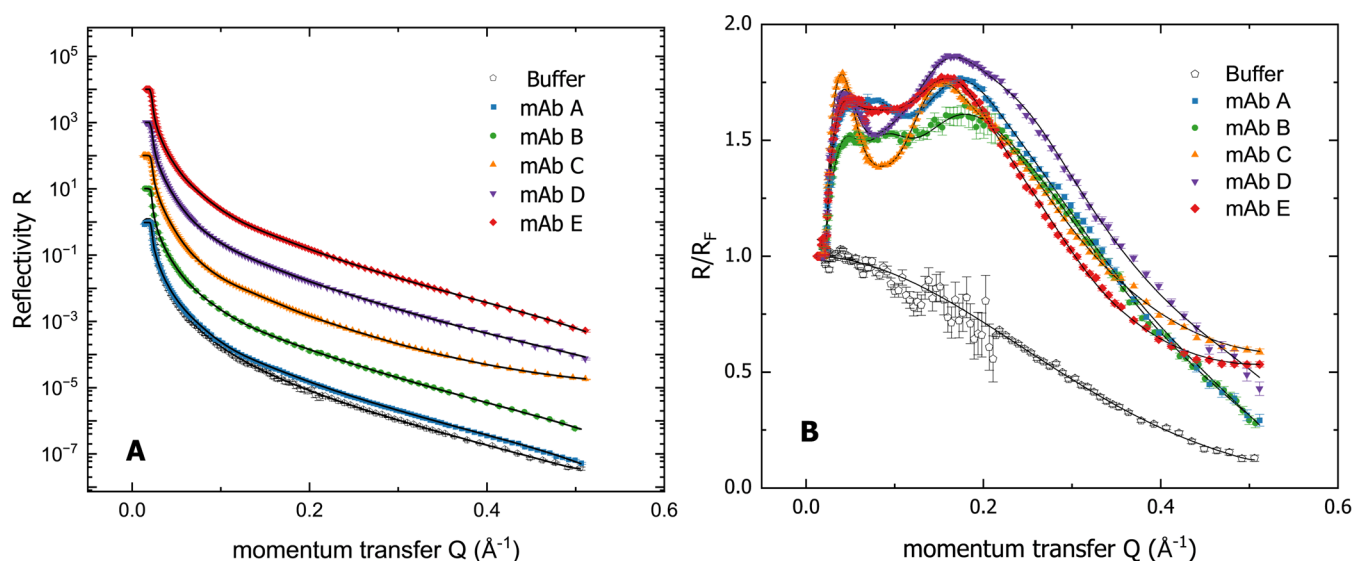


Figure 5. XRR measurements of the air–water interface (buffer) and adsorbed protein layers at the air–water interface at 22 °C. The protein solution concentration is 0.75 mg/mL. (A) Reflectivity curves R of 5 mAbs and buffer and the associated Hermite spline fits (solid lines) as the function of the momentum transfer Q . The reflectivity curves of mAbs B–D were shifted up for clarity (note: $R \rightarrow 1$ as $Q \rightarrow 0$ for all measurements). (B) Fresnel scale R/R_F of the mAbs solutions and buffer solution reflectivity profiles and the Hermite spline fits (solid lines) as a function of momentum transfer vector Q , in which $R/R_F \rightarrow 1$ is $Q \rightarrow 0$. The Fresnel scale is shown to enhance the interfacial features.

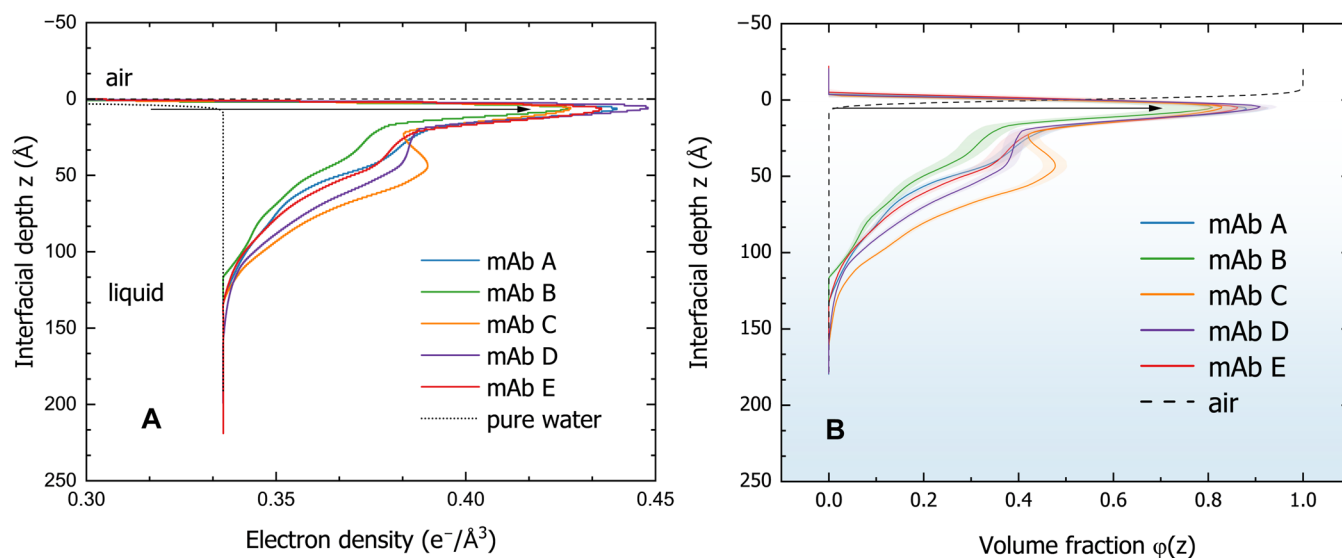


Figure 6. (A) Electron density profile (EDP) from the free-form model fit of the mAb layer as a function of interfacial depth, z . The black dot profile is the theoretical EDP of pure water. Positions $z < 0$ correspond to the air phase and $z > 0$ corresponds to the liquid phase. (B) Volume occupancy profile of five mAbs constructed from the Hermite spline model. The error band represents the 95% confidence band obtained from the Monte Carlo Markov Chain (MCMC) analysis. The dashed line represents the distribution of the air phase. Positions $z > 0$ correspond to the liquid phase region. The high packing density region localized at around $z = 6$ Å below the air phase (indicated by the black arrow) is referred to as the highly hydrophobic region formed by structural rearrangement of mAbs at the air–liquid interface.

between the average “final” interfacial elastic moduli and the $>25 \mu\text{m}$ particle counts is evident in the data plotted in Figure 4B. Within the same class of mAbs, (A, B, C, and E) the data are well correlated by a simple linear relationship with a very significant $R^2 = 0.99$. However, the bispecific antibody D (Table 1) is clearly distinct from this trend with significantly higher moduli that lie well above the data for the other mAb interfaces. As bispecific antibodies have two different Fab regions, this difference in quantitative behavior is not unexpected and the detailed molecular mechanisms for this are left for further investigation.

This empirical correlation between interfacial elastic modulus and $>25 \mu\text{m}$ particle count (Figure 4B) is much more significant than the corresponding correlation with surface pressure (Figure 4A), which reflects the higher sensitivity of interfacial shear rheology to both concentration and interprotein interactions. As a consequence, interfacial shear rheology also distinguishes between the four antibodies and the bispecific antibody D, which presumably has different interprotein interactions at the interface due to its asymmetry.^{42,43} Importantly, the interfacial elastic modulus is much more sensitive as compared to the surface pressure, i.e., the difference in interfacial shear elasticity between the most

stable mAb (mAb B) and the most unstable mAb (mAb A) is 110%, whereas it is only 25% for the corresponding surface pressures. This result shows that the less stable mAbs (A and E) form stronger interfacial films at the air–liquid interface as compared to stable mAbs, as validated by the strong correlation between the long-time formation of visible particles in the formulation and the greater interfacial viscoelasticity of the interface.

3.4. X-ray Reflectometry. To gain a mechanistic understanding of the correlation between surface viscoelasticity and solution long-term stability, XRR measurements were performed on all five mAbs to investigate their interfacial structure and quantify the adsorbed amount. The data are reported as reflectivity, R , versus momentum transfer, Q , shown in Figure 5A, where $Q = (4\pi/\lambda)\sin(\theta)$ and λ is the wavelength of the X-ray radiation. To better highlight the interfacial features of the mAb layer, the XRR data are also presented in the Fresnel scale (R/R_F), where R_F is the Fresnel reflectivity determined for the ideal, zero roughness air–liquid interface (Figure 5B). As seen, for Q values above the critical edge of the air–water interface ($Q_{\text{critical}} \sim 0.0216 \text{ \AA}^{-1}$), the reflectivity profiles for all protein solutions are statistically higher than that of the buffer, which indicates the presence of mAbs at the interface. The Fresnel scale reflectivity curve in Figure 5B shows two main characteristic peaks of mAb at the interface at around $Q = 0.05 \text{ \AA}^{-1}$ and 0.18 \AA^{-1} . These two peaks were also observed in the R/R_F curves of antibodies at a similar bulk concentration reported by Kanthe et al.⁴⁴ The height and width of these characteristic peaks are distinct for each mAb, which suggests differences in the adsorbed conformations at the air–liquid interface.

Analysis of these conformations proceeds by fitting these reflectivity results to electron density profiles normal to the air–water interface using standard methods. Two different approaches were pursued and found to be statistically equivalent, so only the results for the Hermite spline method are shown here, while results for the complementary multislabs model are presented and compared in the SI. In brief, the monotonic Hermite spline model utilized the set of N control points $[(z_0, A_0), \dots, (z_N, A_N)]$ to model the real-space volume occupancy profile. Each control point is initially evenly spaced and allowed to float within small extents from their original position.²¹ A Monte Carlo Markov Chain (MCMC) optimizer is also used to obtain unbiased modeling uncertainties.^{21,22} Both fitting models yield nearly identical electron density profiles (EDPs) for each mAb (as shown in Figure S7 of the Supporting Information), confirming the uniqueness of the EDP of each mAb at the air–liquid interface. The EDP of all 5 antibodies is shown in Figure 6A. As the EDP transitions from the air phase to the liquid, for all mAbs, the EDP peak around $z = 6 \text{ \AA}$ has a peak electron density greater than $0.42 \text{ e}^-/\text{\AA}^3$. Then, the EDPs of mAb A, B, D, and E monotonically decay to reach the electron density of water of $0.336 \text{ e}^-/\text{\AA}^3$. mAb C, on the other hand, exhibits a secondary peak at around $z = 50 \text{ \AA}$, followed by a decay to the electron density of water.

Similar electron densities were also observed from studies by Kanthe et al.^{14,44} The high electron density peak at $z = 6 \text{ \AA}$ for all mAbs was identified and suggested to be indicative of β -sheet formation between mAbs adsorbed at the air–water interface.¹⁴ For the EDP curves in Figure 6A, the value of z where the density profile starts to reach the electron density of water indicates the thickness of the mAb interfacial layer. The integrated area under the protein EDP and the water electron

density is the total electron density per area of each mAb in the adsorbed region, which is proportional to the amount of adsorbed protein. The difference in this integrated area among the mAbs can be visualized in Figure 6A, indicating a different adsorbed amount for each mAb at the air–water interface. The calculated adsorbed protein total volume fractions are tabulated in Table 1.

The volume occupancy (VO) profile, as shown in Figure 6B, provides a direct indication of the molecular orientation of proteins adsorbed at the interface. This volume occupancy profile was constructed directly from the Hermite spline model fitting or derived from the electron density profile (from the slab model) by the continuous spatial distribution model as described by Shekhar et al.^{21,45} Similar to the electron density profiles in Figure 6A, in the VO profiles, at $z = 6 \text{ \AA}$, a dense-packing region of all proteins (indicated by the black arrow) is observed. This region has high packing density, with protein volume fraction, φ , varying between 0.8 and 0.9, which have been suggested as β -sheet structures stemming from the conformational change of mAbs at the air–water interface as discussed by Kanthe et al.¹⁴ This high volume fraction density near the air phase was also observed in the VO profiles for β -casein and β -lactoglobulin at the air–water interface.⁴⁶ The volume fraction of water in this region ranges from 0.1 to 0.2, which indicates a high hydrophobicity in this region. Therefore, it is reasonable to suppose that this high density, hydrophobic region promotes *in situ* hydrophobic interactions that cannot be quantified by hydrophobic interaction chromatography (HIC) as discussed by Shieh et al.¹¹ The presence of this hydrophobic region probed by XRR among proteins also agrees with the increase in hydrophobicity of protein layers at the air–water interface compared to the bulk as reported by Anderson et al. and Leiske et al.^{47,48}

Comparing the volume occupancy profiles among antibodies suggests subtle differences in the adsorbed mAb conformations at the air–water interface. It is notable that mAb C has a secondary peak on the volume fraction profile at $z = 50 \text{ \AA}$, which is not observed in the other protein volume profiles. This implies a difference in the molecular orientation of mAb C adsorbed at the interface as compared with the other mAbs, which may be associated with unique, nonmonotonic time evolution of the interfacial elastic modulus G'_e presented in Figure 3a. Further work is necessary to investigate this observation, such as molecular simulations of the adsorbed structure and interfacial rheology, which is beyond the scope of this manuscript. For reference, the VO profiles of several simple, possible mAb orientations at the interface are presented in Figure S9 (Supporting Information).

At hydrophobic interfaces such as the air–water interface, proteins are believed to undergo conformational change to expose hydrophobic residues to the hydrophobic phase (i.e., air in this system) and lower overall free energy.^{48,49} This structural rearrangement leads to enhancement in hydrophobic interactions with the tightly packed, neighboring molecules, giving rise to the β -sheet formation, as has been confirmed for some hydrophobins and monoclonal antibodies.^{14,50} As discussed, the interfacial elastic (or storage) modulus is a metric to quantify the interprotein interaction at the air–water interface, which could reflect the long-term instability (or particulate formation propensity) of antibodies in solution.³⁶ Thus, it is reasonable to interpret the enhancement in interprotein interactions at the interface as probed by interfacial rheology as being due to strong interprotein

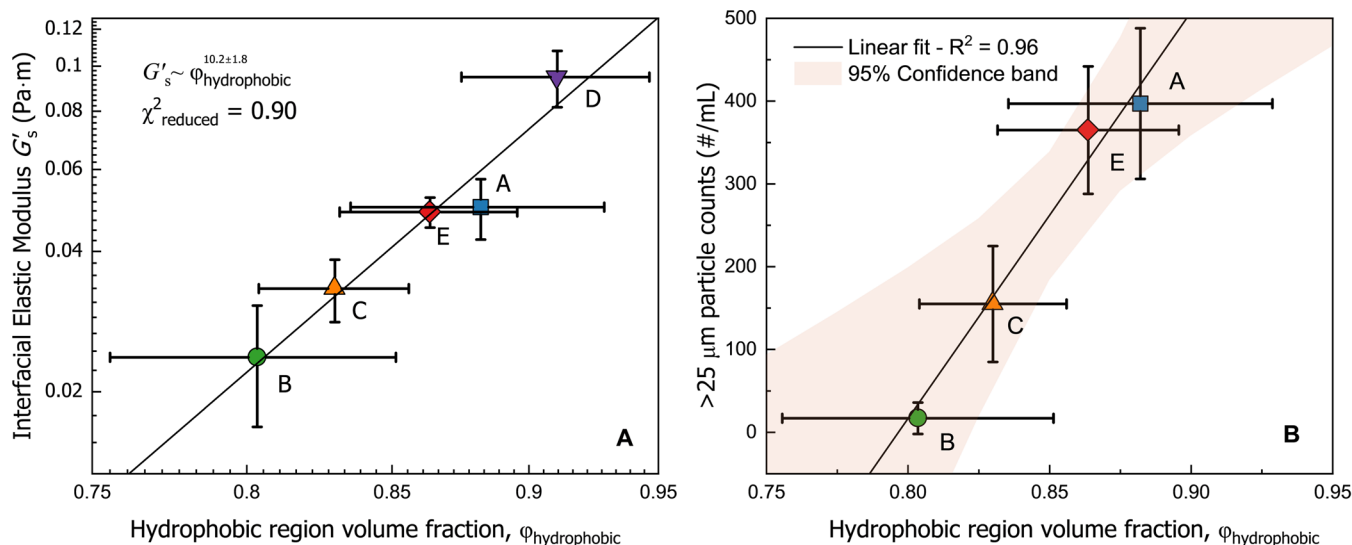


Figure 7. (A) Interfacial elastic modulus G'_s follows a strong exponential scaling with an exponent of 10.2 ± 1.8 with the volume fraction of proteins in the hydrophobic region at the interface. (B) Observation of visible particle counts also correlates with the protein concentration in this hydrophobic region at the interface, showing a linear correlation with an R^2 of 0.96.

hydrophobic attractions, such as β -sheet formation, as indicated by significant enhancement in protein concentration in the hydrophobic region at the air interface, as shown by the strong peak in the XRR measurements. Indeed, the interfacial elastic modulus G'_s follows a strong exponential scaling with an exponent of 10.2 ± 1.8 with the volume fraction of proteins in the hydrophobic region at the interface as demonstrated in Figure 7A. An exponential dependence of the elastic modulus is observed in concentrated colloidal gels and glasses as described elsewhere.^{34,36} Naturally then, the observation of visible particle counts also correlates with the protein concentration in this hydrophobic region at the interface, showing a linear correlation with an R^2 of 0.96 as shown in Figure 7B. The total amount of absorbed protein (i.e., the total volume fraction of mAb at the interface) also correlates with the interfacial elastic modulus and visible particle counts, as shown in Figure S8 (Supporting Information). However, these correlations with the total adsorbed amount are not as strong as the correlation with the strong enhancement of protein concentration in the hydrophobic region. Although the stability study and interfacial characterizations were conducted at different temperatures, i.e., one at 5 °C and the others at 22 ± 2 °C; as it is more practical to perform air–water interface characterization (surface tensiometry, rheology, and reflectivity) at room temperature, it is reasonable to believe the validity of these correlations. To elaborate, within the time scale of all surface measurements (less than 10 h), the thermodynamics of the protein interface could be described by Gibbs isotherms^{17,51} and the Arrhenius law is still applicable for the kinetics as described elsewhere.¹⁷ The interprotein interaction at the interface is likely to be dominated by hydrophobic interactions, which systematically scale over the temperature range 0–80 °C.⁵² Moreover, it is important to note that all of the experiment temperatures (5–22 °C) are all below the onset melting temperature of monoclonal antibodies, which is approximately greater than 55 °C,⁵³ such that the change in temperature should not significantly perturb the native structure. Thus, while interfacial properties are temperature-dependent, we can reasonably expect the results to scale similarly with temperature across the series of mAbs.

These results suggest the mechanistic connection among interfacial structure, rheology, and long-term stability of antibodies in formulation; i.e., the mAbs that form a greater number of visible aggregates in solution also form stronger mechanical films at that air–water interface as both may be promoted by hydrophobic interactions. Thus, the long-term aggregation in mAb formulations over years of observation is presumed to be catalyzed by the highly concentrated and oriented mAbs at the hydrophobic air–liquid interface, enabling the probing of particulate formation propensity within hours via interfacial rheology.

4. CONCLUSIONS

In summary, we confirm the hypothesis of a strong correlation between interfacial shear elastic moduli at the air–water interface and the long-term formation of visible particles in the formulation for a specific class of mAbs. The interfacial elastic modulus is much more sensitive in distinguishing between mAbs that show such undesired instability in formulations as compared to surface pressure measurements. And, while the surface pressure correlates with long-term formulation instability across all five mAbs probed, the surface viscoelasticity not only shows a strong correlation *within* a broad class of mAbs but can also clearly distinguish the bispecific antibody among those tested. Thus, we validate the hypothesis that mAbs with a higher solution particulate formation propensity form interfacial films with higher interfacial shear elasticity at the air–water interface. XRR data provide partial molecular justification for this correlation by revealing the presence of a high density region of mAb directly at the hydrophobic air–water interface that has been associated with the interprotein β -sheet formation. The interfacial shear elasticity increases exponentially with this local interfacial protein volume fraction, which then correlates directly with the long-term formation of visible particles. This new structure–property relationship provides partial mechanistic insights into the correlation between the interfacial rheology and long-term stability of the protein solution. This new correlation is of practical value as one possible metric for screening biopharmaceutical formulations in the early stage of

development. Further research on characterizing the microstructures of aggregates in solution and the impact of salts on the interfacial properties will help verify and broaden the use of rheology in predicting particulate formation propensity of antibodies in formulation.

■ ASSOCIATED CONTENT

SI Supporting Information

The Supporting Information is available free of charge at <https://pubs.acs.org/doi/10.1021/acs.jpcb.3c05900>.

Materials & Long-term stability study; Rheology Characterization; and X-ray Reflectivity and Surfactant Effects on Interfacial Properties (PDF)

■ AUTHOR INFORMATION

Corresponding Authors

Ken K. Qian – Eli Lilly and Company, Indianapolis, Indiana 46225, United States; Email: qian_ken_k@lilly.com

Norman J. Wagner – Department of Chemical & Biomolecular Engineering, Center for Neutron Science, University of Delaware, Delaware 19716, United States; orcid.org/0000-0001-9565-619X; Email: wagnernj@udel.edu

Authors

Kiet G. Pham – Department of Chemical & Biomolecular Engineering, Center for Neutron Science, University of Delaware, Delaware 19716, United States; orcid.org/0000-0003-1580-6632

Benjamin R. Thompson – Department of Chemical & Biomolecular Engineering, Center for Neutron Science, University of Delaware, Delaware 19716, United States; orcid.org/0000-0002-8309-9522

Tingting Wang – Eli Lilly and Company, Indianapolis, Indiana 46225, United States

Shayak Samaddar – Eli Lilly and Company, Indianapolis, Indiana 46225, United States

Yun Liu – Department of Chemical & Biomolecular Engineering, Center for Neutron Science, University of Delaware, Delaware 19716, United States; NIST Center for Neutron Research, National Institute of Standards and Technology, Gaithersburg, Maryland 20899, United States; orcid.org/0000-0002-0944-3153

Complete contact information is available at: <https://pubs.acs.org/doi/10.1021/acs.jpcb.3c05900>

Notes

The authors declare no competing financial interest.

■ ACKNOWLEDGMENTS

The therapeutics protein materials for this work were supplied by Eli Lilly and Company. This work was supported by funding from Eli Lilly and Company. The authors would like to thank Dr. Sushil Satija and Dr. Minh Phan for helping with the XRR measurements conducted at the National Institute of Standards and Technology and Dr. Guangcui Yuan and Dr. Frank Heinrich for assistance with reducing and analyzing XRR measurements. Certain commercial equipment, instruments, or materials (or suppliers, or software, etc.) are identified in this paper to foster understanding. Such identification does not imply recommendation or endorsement by the National Institute of Standards and Technology, nor does it imply

that the materials or equipment identified are necessarily the best available for the purpose.

■ REFERENCES

- (1) Elvin, J. G.; Couston, R. G.; van der Walle, C. F. Therapeutic antibodies: market considerations, disease targets and bioprocessing. *Int. J. Pharm.* **2013**, *440* (1), 83–98.
- (2) Roberts, C. J. Therapeutic protein aggregation: mechanisms, design, and control. *Trends Biotechnol.* **2014**, *32* (7), 372–380.
- (3) Carpenter, J. F.; Randolph, T. W.; Jiskoot, W.; Crommelin, D. J. A.; Middaugh, C. R.; Winter, G.; Fan, Y. X.; Kirshner, S.; Verthelyi, D.; Kozlowski, S.; et al. Overlooking Subvisible Particles in Therapeutic Protein Products: Gaps That May Compromise Product Quality. *J. Pharm. Sci.* **2009**, *98* (4), 1201–1205.
- (4) Kuzman, D.; Bunc, M.; Ravnik, M.; Reiter, F.; Zagar, L.; Boncina, M. Long-term stability predictions of therapeutic monoclonal antibodies in solution using Arrhenius-based kinetics. *Sci. Rep.* **2021**, *11* (1), No. 20534.
- (5) Barnett, G. V.; Razinkov, V. I.; Kerwin, B. A.; Hillsley, A.; Roberts, C. J. Acetate- and Citrate-Specific Ion Effects on Unfolding and Temperature-Dependent Aggregation Rates of Anti-Streptavidin IgG1. *J. Pharm. Sci.* **2016**, *105* (3), 1066–1073.
- (6) Weiss, W. F.; Young, T. M.; Roberts, C. J. Principles, approaches, and challenges for predicting protein aggregation rates and shelf life. *J. Pharm. Sci.* **2009**, *98* (4), 1246–1277.
- (7) Wang, W.; Roberts, C. J. Non-Arrhenius protein aggregation. *AAPS J.* **2013**, *15* (3), 840–851.
- (8) Moorthy, B. S.; Schultz, S. G.; Kim, S. G.; Topp, E. M. Predicting protein aggregation during storage in lyophilized solids using solid state amide hydrogen/deuterium exchange with mass spectrometric analysis (ssHDX-MS). *Mol. Pharmaceutics* **2014**, *11* (6), 1869–1879.
- (9) Chennamsetty, N.; Voynov, V.; Kayser, V.; Helk, B.; Trout Bernhardt, L. Design of therapeutic proteins with enhanced stability. *Proc. Natl. Acad. Sci. U.S.A.* **2009**, *106* (29), 11937–11942.
- (10) Roberts, C. J.; Das, T. K.; Sahin, E. Predicting solution aggregation rates for therapeutic proteins: approaches and challenges. *Int. J. Pharm.* **2011**, *418* (2), 318–333.
- (11) Shieh, I. C.; Patel, A. R. Predicting the Agitation-Induced Aggregation of Monoclonal Antibodies Using Surface Tensiometry. *Mol. Pharmaceutics* **2015**, *12* (9), 3184–3193.
- (12) Mitropoulos, V.; Mütze, A.; Fischer, P. Mechanical properties of protein adsorption layers at the air/water and oil/water interface: A comparison in light of the thermodynamical stability of proteins. *Adv. Colloid Interface Sci.* **2014**, *206*, 195–206.
- (13) Petkov, J. T.; Gurkov, T. D.; Campbell, B. E.; Borwankar, R. P. Dilatational and Shear Elasticity of Gel-like Protein Layers on Air/Water Interface. *Langmuir* **2000**, *16* (8), 3703–3711.
- (14) Kanthe, A.; Ilott, A.; Krause, M.; Zheng, S.; Li, J.; Bu, W.; Bera Mrinal, K.; Lin, B.; Maldarelli, C.; Tu Raymond, S. No ordinary proteins: Adsorption and molecular orientation of monoclonal antibodies. *Sci. Adv.* **2022**, *7* (35), No. eabg2873.
- (15) Ruane, S.; Li, Z.; Hollowell, P.; Hughes, A.; Warwicker, J.; Webster, J. R. P.; van der Walle, C. F.; Kalonia, C.; Lu, J. R. Investigating the Orientation of an Interfacially Adsorbed Monoclonal Antibody and Its Fragments Using Neutron Reflection. *Mol. Pharmaceutics* **2023**, *20* (3), 1643–1656.
- (16) Tein, Y. S.; Zhang, Z.; Wagner, N. J. Competitive Surface Activity of Monoclonal Antibodies and Nonionic Surfactants at the Air–Water Interface Determined by Interfacial Rheology and Neutron Reflectometry. *Langmuir* **2020**, *36* (27), 7814–7823.
- (17) Kanthe, A. D.; Tu, R.; Maldarelli, C. Protein Adsorption at a Gas-Aqueous Interface. In *Protein Instability at Interfaces During Drug Product Development: Fundamental Understanding, Evaluation, and Mitigation*, Li, J.; Krause, M. E.; Tu, R., Eds.; Springer International Publishing, 2021; pp 9–49.
- (18) Vandebril, S.; Franck, A.; Fuller, G. G.; Moldenaers, P.; Vermant, J. A double wall-ring geometry for interfacial shear rheometry. *Rheol. Acta* **2010**, *49* (2), 131–144.

- (19) Maranville, B.; Ratcliff II, W.; Kienzle, P. reductus: a stateless Python data reduction service with a browser front end. *J. Appl. Crystallogr.* **2018**, *51* (5), 1500–1506. Kienzle, P. A. O. D.; K, V.; Ankner, J. F.; Berk, N. F.; Majkrzak, C. *NCNR Reflectometry Software* <https://www.nist.gov/ncnr/data-reduction-analysis/reflectometry-software> (accessed March 5, 2023).
- (20) Zhang, Z.; Orski, S.; Woys, A. M.; Yuan, G.; Zarraga, I. E.; Wagner, N. J.; Liu, Y. Adsorption of polysorbate 20 and proteins on hydrophobic polystyrene surfaces studied by neutron reflectometry. *Colloids Surf., B* **2018**, *168*, 94–102.
- (21) Heinrich, F.; Losche, M. Zooming in on disordered systems: neutron reflection studies of proteins associated with fluid membranes. *Biochim. Biophys. Acta, Biomembr.* **2014**, *1838* (9), 2341–2349.
- (22) Kirby, B. J.; Kienzle, P. A.; Maranville, B. B.; Berk, N. F.; Krycka, J.; Heinrich, F.; Majkrzak, C. F. Phase-sensitive specular neutron reflectometry for imaging the nanometer scale composition depth profile of thin-film materials. *Curr. Opin. Colloid Interface Sci.* **2012**, *17* (1), 44–53.
- (23) Bollenbach, L.; Buske, J.; Mader, K.; Garidel, P. Poloxamer 188 as surfactant in biological formulations - An alternative for polysorbate 20/80? *Int. J. Pharm.* **2022**, *620*, No. 121706.
- (24) Kannan, A.; Shieh, I. C.; Fuller, G. G. Linking aggregation and interfacial properties in monoclonal antibody-surfactant formulations. *J. Colloid Interface Sci.* **2019**, *550*, 128–138.
- (25) Zhang, Z.; Marie Woys, A.; Hong, K.; Grapentin, C.; Khan, T. A.; Zarraga, I. E.; Wagner, N. J.; Liu, Y. Adsorption of non-ionic surfactant and monoclonal antibody on siliconized surface studied by neutron reflectometry. *J. Colloid Interface Sci.* **2021**, *584*, 429–438.
- (26) Dixit, N.; Maloney, K. M.; Kalonia, D. S. Protein-silicone oil interactions: comparative effect of nonionic surfactants on the interfacial behavior of a fusion protein. *Pharm. Res.* **2013**, *30* (7), 1848–1859.
- (27) Grapentin, C.; Muller, C.; Kishore, R. S. K.; Adler, M.; ElBialy, I.; Friess, W.; Huwyler, J.; Khan, T. A. Protein-Polydimethylsiloxane Particles in Liquid Vial Monoclonal Antibody Formulations Containing Poloxamer 188. *J. Pharm. Sci.* **2020**, *109* (8), 2393–2404.
- (28) Kannan, A.; Shieh, I. C.; Leiske, D. L.; Fuller, G. G. Monoclonal Antibody Interfaces: Dilatation Mechanics and Bubble Coalescence. *Langmuir* **2018**, *34* (2), 630–638. Kannan, A.; Shieh, I. C.; Hristov, P.; Fuller, G. G. In-Use Interfacial Stability of Monoclonal Antibody Formulations Diluted in Saline i.v. Bags. *J. Pharm. Sci.* **2021**, *110* (4), 1687–1692.
- (29) Kannan, A.; Shieh, I. C.; Negulescu, P. G.; Chandran Suja, V.; Fuller, G. G. Adsorption and Aggregation of Monoclonal Antibodies at Silicone Oil–Water Interfaces. *Mol. Pharmaceutics* **2021**, *18* (4), 1656–1665.
- (30) Hua, X.Y.; Rosen, M. J. Dynamic surface tension of aqueous surfactant solutions: I. Basic parameters. *J. Colloid Interface Sci.* **1988**, *124* (2), 652–659.
- (31) Lin, G. L.; Pathak, J. A.; Kim, D. H.; Carlson, M.; Riguerro, V.; Kim, Y. J.; Buff, J. S.; Fuller, G. G. Interfacial dilatational deformation accelerates particle formation in monoclonal antibody solutions. *Soft Matter* **2016**, *12* (14), 3293–3302.
- (32) Jaensson, N. O.; Anderson, P. D.; Vermant, J. Computational interfacial rheology. *J. Non-Newtonian Fluid Mech.* **2021**, *290*, No. 104507.
- (33) Hermans, E.; Saad Bhamla, M.; Kao, P.; Fuller, G. G.; Vermant, J. Lung surfactants and different contributions to thin film stability. *Soft Matter* **2015**, *11* (41), 8048–8057.
- (34) Mewis, J.; Wagner, N. J. *Colloidal Suspension Rheology*; Cambridge University Press, 2011; Vol. 393. DOI: 10.1017/CBO9780511977978.
- (35) Renggli, D.; Aliche, A.; Ewoldt, R. H.; Vermant, J. Operating windows for oscillatory interfacial shear rheology. *J. Rheol.* **2020**, *64* (1), 141–160.
- (36) Wood, C. V.; Razinkov, V. I.; Qi, W.; Roberts, C. J.; Vermant, J.; Furst, E. M. Antibodies Adsorbed to the Air–Water Interface Form Soft Glasses. *Langmuir* **2023**, *39* (22), 7775–7782.
- (37) Ghebremedhin, M.; Seiffert, S.; Vilgis, T. A. Physics of agarose fluid gels: Rheological properties and microstructure. *Curr. Res. Food Sci.* **2021**, *4*, 436–448.
- (38) Wen, Y. H.; Schaefer, J. L.; Archer, L. A. Dynamics and Rheology of Soft Colloidal Glasses. *ACS Macro Lett.* **2015**, *4* (1), 119–123.
- (39) Aliche, A.; Simon, S.; Sjoblom, J.; Vermant, J. Assessing the Interfacial Activity of Insoluble Asphaltene Layers: Interfacial Rheology versus Interfacial Tension. *Langmuir* **2020**, *36* (49), 14942–14959.
- (40) Smith, C.; Li, Z.; Holman, R.; Pan, F.; Campbell, R. A.; Campana, M.; Li, P.; Webster, J. R.; Bishop, S.; Narwal, R.; et al. Antibody adsorption on the surface of water studied by neutron reflection. *MAbs* **2017**, *9* (3), 466–475.
- (41) Commereuc, S. Basic Rheology of Polymer Melts. An Introductory Polymer Science Experiment. *J. Chem. Educ.* **1999**, *76* (11), 1528.
- (42) Jay, J. W.; Bray, B.; Qi, Y.; Igbinigie, E.; Wu, H.; Li, J.; Ren, G. IgG Antibody 3D Structures and Dynamics. *Antibodies* **2018**, *7* (2), 18.
- (43) Kapelski, S.; Cleiren, E.; Attar, R. M.; Philippar, U.; Hasler, J.; Chiu, M. L. Influence of the bispecific antibody IgG subclass on T cell redirection. *MAbs* **2019**, *11* (6), 1012–1024.
- (44) Kanthe, A. D.; Krause, M.; Zheng, S.; Ilott, A.; Li, J.; Bu, W.; Bera, M. K.; Lin, B.; Maldarelli, C.; Tu, R. S. Armoring the Interface with Surfactants to Prevent the Adsorption of Monoclonal Antibodies. *ACS Appl. Mater. Interfaces* **2020**, *12* (8), 9977–9988.
- (45) Shekhar, P.; Nanda, H.; Losche, M.; Heinrich, F. Continuous distribution model for the investigation of complex molecular architectures near interfaces with scattering techniques. *J. Appl. Phys.* **2011**, *110* (10), 102216–10221612.
- (46) Atkinson, P. J.; Dickinson, E.; Horne, D. S.; Richardson, R. M. Neutron reflectivity of adsorbed β -casein and β -lactoglobulin at the air/water interface. *J. Chem. Soc., Faraday Trans.* **1995**, *91* (17), 2847–2854.
- (47) Leiske, D. L.; Shieh, I. C.; Tse, M. L. A Method To Measure Protein Unfolding at an Air-Liquid Interface. *Langmuir* **2016**, *32* (39), 9930–9937.
- (48) Anderson, R. E.; Pande, V. S.; Radke, C. J. Dynamic lattice Monte Carlo simulation of a model protein at an oil/water interface. *J. Chem. Phys.* **2000**, *112* (20), 9167–9185.
- (49) Yano, Y. F. Kinetics of protein unfolding at interfaces. *J. Phys.: Condens. Matter* **2012**, *24* (50), No. 503101.
- (50) Kwan*, A. H. Y.; W, R. D.; Sunde, M.; Matthews, J. M.; Haverkamp, R. G.; Templeton†, M. D.; Mackay, J. P. Structural basis for rodlet assembly in fungal hydrophobins. *Proc. Natl. Acad. Sci. U.S.A.* **2006**, *103*, 3621–3626.
- (51) Wang, Y.; Wang, T.; Chen, Q.; Zhou, W.; Guo, J. Correlation between the Protein Pharmaceutical Surface Activity and Interfacial Stability. *Mol. Pharmaceutics* **2023**, *20* (5), 2536–2544.
- (52) Sun, Q.; Fu, Y.; Wang, W. Temperature effects on hydrophobic interactions: Implications for protein unfolding. *Chem. Phys.* **2022**, *559*, No. 111550.
- (53) Thiagarajan, G.; Semple, A.; James, J. K.; Cheung, J. K.; Shameem, M. A comparison of biophysical characterization techniques in predicting monoclonal antibody stability. *MAbs* **2016**, *8* (6), 1088–1097.